Nuclear Engineering and Technology 53 (2021) 2126–2132

Contents lists available at ScienceDirect

Nuclear Engineering and Technology

journal homepage: www.elsevier.com/locate/net

Original Article

Design and neutronic analysis of the intermediate heat exchanger of a fast-spectrum molten salt reactor

Jamiyansuren Terbish [a, *], W.F.G. van Rooijen [b]

[a] Nuclear Research Center, National University of Mongolia, Ulaanbaatar, Mongolia
[b] Research Institute of Nuclear Engineering, University of Fukui, Tsuruga, Japan

ARTICLE INFO

Article history:
Received 17 September 2020
Received in revised form
26 December 2020
Accepted 22 January 2021
Available online 29 January 2021

Keywords:
Molten salt reactor
Intermediate heat exchanger
Neutronic analysis

ABSTRACT

Various research groups and private interprises are pursuing the design of a Molten Salt Reactor (MSR) as one of the Generation-IV concepts. In the current work a fast neutron MSR using chloride fuel is analyzed, specially analyzing the power production and neutron flux level in the Intermediate Heat Exchanger (IHX). The neutronic analysis in this work is based on a chloride-fuel MSR with 600 MW thermal power. The core power density was set to 100 MW m −3 with a core H/D [[EQUATION]] 1.0 amd four Intermediate Heat Exchanger (IHX). This leads to a power of 150 MW per IHX; this power is also comparable to the IHX proposed in the SAMOFAR framework. In this work, a preliminary design of a 150 MW helical-coil IHX for a chloride-fueled MSR is prepared and the fission rate, capture rate, and inelastic scatter rate are evaluated.

1. Introduction

Various research groups and private enterprises are pursuing the design of a Molten Salt Reactor (MSR) as one of the Generation-IV concepts. In the current work a fast neutron MSR using chloride fuel is analyzed, specifically analyzing the power production and neutron flux level in the Intermediate Heat Exchanger (IHX). Chloride salt was selected because the solubility of actinides in chloride salt is high and the melting point is relatively low [1,2]. Due to the high solubility of actinides in chloride salt, a fast spectrum MSR is possible while maintaining a relatively small core size. Such a fast-spectrum MSR does not have a moderator in the core, leading to a simple core structure, where criticality of the fuel mixture is basically dictated by the geometry of the core vessel. In recent years, a fast-spectrum fluoride-based MSR was analyzed in detail in the SAMOFAR project [3,4].

The main impetus for the present analysis is as follows: the process of nuclear fission leads to the production of a small amount of so-called *precursor nuclei*; a precursor nucleus emits a neutron by radioactive decay (these are the so-called *delayed neutrons*). In the case of an MSR, the fuel circulates throughout the primary system, and thus the entire primary circuit contains a neutron source due to the decay of the precursors. The MSR considered in this work is a fast spectrum reactor. Such a reactor does not contain a moderator in the core, and thus criticality is determined only by the geometry of the core vessel. This means that basically, the entire primary system outside of the core region is one big sub-critical multiplying system. Thus there is power production in the entire primary system, and due to the size and shape, the multiplication of neutrons in the heat exchangers could be considerable. In this work a neutronic analysis is performed to assess the fission power level and neutron flux in the heat exchangers.

The neutronic analysis in this work is based on a chloride-fuel MSR with 600 MW thermal power (Table 1). The core power density was set to 100MWm^{-3} with a core H/D-ratio of ≈ 1.0 and four Intermediate Heat Exchangers (IHX). This leads to a power of 150 MW per IHX; this power is also comparable to the IHX proposed in the SAMOFAR framework [5]. In this work, a preliminary design of a 150 MW helical-coil IHX for a chloride-fueled MSR is prepared and the fission rate, capture rate, and inelastic scatter rate are evaluated. The organization of this paper is as follows: in Section 2 the design of the IHX for the chloride fuel is discussed, and in Section 3 the neutronic modeling is discussed. In Section 4 the results are presented and the paper closes with a section of conclusions and discussion (Section 5).

* Corresponding author.
E-mail address: t.jamiyansuren@num.edu.mn (J. Terbish).

https://doi.org/10.1016/j.net.2021.01.021

Table 1
Boundary conditions for the Molten Salt Reactor and Intermediate Heat Exchanger.

Quantity	Value
Core and primary system	
Power	600 MW
Core height	190 cm
Core radius	100 cm
Core H/D ratio	0.95
Core volume	5.97m^3
Fuel mass flow rate	9231 kg s^{-1}
Core traversal time	2.1s
Core power density	100MWm^{-3}
IHX	
Unit power	150 MW
Fuel side inlet temperature $T_{h,i}$	650 °C
Fuel side outlet temperature $T_{h,o}$	550 °C
Coolant side inlet temperature $T_{c,i}$	500 °C
Fuel side outlet temperature $T_{c,o}$	575 °C
General	
Structural material	SS-316

2. Design of the intermediate heat exchanger

The boundary conditions for the design of the intermediate heat exchanger are given in Table 1. The fuel is molten salt of composition $NaCl-CaCl_2-UCl_3-PuCl_3$ (molar fractions 35%–35% - 22.5%–7.5%, melt point around 541 °C (=714 K) [6]), the coolant is a eutectic mixture $KCl-MgCl_2$ (molar fractions 67%–33%, melt point 435 °C [7]). Material properties of the fuel and the coolant were calculated (and in some cases estimated) based on various sources [1,7–10]. The reference values adopted in this work are listed in Table 2. Stainless steel 316 is selected as the structural material. It is realized that SS-316 is probably not applicable for this kind of reactor due to corrosion properties, but for the neutronic calculations SS-316 represents a reasonable composition of the structural material, and for thermal-hydraulic design SS-316 represents a reasonable thermal conductivity.

The design was prepared taking the following steps: a helical coil design is adopted. The helical coil design is expected to give good performance with a small IHX volume. The fuel is on the shell side (fluid outside of the heat exchanger tubes) and flows from top to bottom. The secondary coolant is on the tube side (inside the heat exchanger tubes) and flows from bottom to top to make a counterflow heat exchanger. The $\varepsilon-$NTU method [5,11] was used to determine the required UA of the heat exchanger, where U is the average heat exchange coefficient and A is the heat exchanging surface area. For a counterflow heat exchanger:

$$\mathrm{NTU}=\frac{1}{C_r-1}\ln\left(\frac{\varepsilon-1}{\varepsilon C_r-1}\right) \tag{1}$$

with

Table 2
Reference data pertaining to the molten salts in this work.

Quantity	Value
Density (fuel, g cm^{-3})	$\rho(T)=3.979-8.640\times10^{-4}T$
Density (coolant, g cm^{-3})	$\rho(T)=2.080-4.835e\times10^{-4}T$
Heat capacity (fuel, J kg^{-1} K^{-1})	$c_p=614$
Heat capacity (coolant, J kg^{-1} K^{-1})	$c_p=1100$
Viscosity (fuel), Pa s	$\eta=0.0544e^{(3880.0/T)}$
Viscosity (coolant), Pa s	$\eta=1.408\times10^{-4}e^{(2261.3/T)}$

$$\varepsilon\equiv\frac{T_{h,i}-T_{h,o}}{T_{h,i}-T_{c,i}} \tag{2}$$

with $T_{h,i}, T_{h,o}$ the inlet and outlet temperature on the hot side and $T_{c,i}$ the inlet temperature on the cold side; $C_r\equiv C_{\min}/C_{\max}$ where C indicates the heat capacity rate, i.e. for the fluid on the hot side $C_h=\dot{m}_h c_{p,h}$ and for the cold side $C_c=\dot{m}_c c_{p,c}$. A standard tube size was selected for the heat exchanger tubes ([12]): tube outside diameter $D_o=12.7$mm and wall thickness $t_w=1.2$mm. Given the mass flow of coolant and the flow area of one tube, the minimum number of tubes is calculated taking into account that the coolant flow velocity inside the tubes should not exceed $v_{\max}=5\mathrm{ms}^{-1}$. It is assumed that the tubes are arranged into 4 sets, where each set is connected through a header to the secondary coolant loop. The tubes are arranged in a square lattice on the header with horizontal and vertical spacing $\delta x=\delta y=1.25D_o$. Thus each header has a rectangular lattice of $NX\times NY$ tube connections. Thus the size of the tube sheet on one header is $NX.\delta x$ wide and $NY.\delta y$ high; the tubes then form a helix with a vertical pitch such that the tube bundle from one header clears the next header.

The heat transfer coefficient inside the tubes h_t is calculated with the Dittus-Boelter relation for the Nusselt number:

$$\mathrm{Nu}=0.023\mathrm{Re}^{0.8}\mathrm{Pr}^{0.4} \tag{3}$$

For simplicity, it assumed that the mass flow is the same in each tube. On the shell side, the heat exchange coefficient h_s is determined using the Nusselt number calculated with the correlation proposed by Zukauskas for a bank of tubes arranged in a square lattice in cross flow [13]:

$$\mathrm{Nu}=0.27\mathrm{Re}^{0.63}\mathrm{Pr}^{0.36}\left(\frac{\mathrm{Pr}}{\mathrm{Pr}_w}\right)^{0.25} \tag{4}$$

where the dimensionless numbers are calculated based on the flow velocity in the minimum free cross section between the tubes ($S_{\min}$ in Fig. 1) and the tube outer diameter D_o. The overall heat exchange

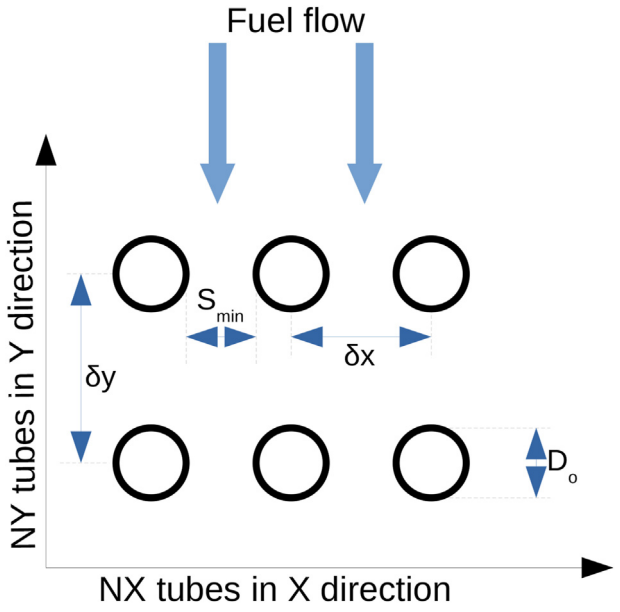

Fig. 1. Illustration of the rectangular arrangement of the tubes showing the horizontal and vertical pitches δx and δy, the tube outer diameter D_o and the minimal flow window size $S_{\min}$.

coefficient is calculated as:

$$\frac{1}{UA}=\frac{1}{A_s h_s}+\frac{1}{A_t h_t}+\frac{\ln(D_o/D_i)}{2\pi L\lambda} \tag{5}$$

where A_s is the heat exchanging surface on the shell side, A_t is the heat exchanging surface on the tube side, L is the total length of the tubes and λ is the thermal conductivity of the tube material.

3. Neutronic analysis

The objective of the neutronic analysis is to determine the neutron flux level, fission reaction rate and related parameters in the IHX. The specific property of Molten Salt Reactors is that the fuel is liquid and traverses the entire primary system. The fission process leads to the production of delayed neutron precursor nuclei. The precursors decay throughout the primary system, thereby causing a distributed source of neutrons throughout the primary system, and as a result, there is a non-zero neutron flux, and a non-zero fission rate, and thus some power production, throughout the primary system. The goal is to determine the neutron flux, fission rate and power production in the IHX.

The neutronic analysis is based on the following simplified model. Consider that the primary circuit is subdivided into a number of regions; give each region an index number i. Such a volume could be the inlet plenum of the IHX, the tube-bundle region of the IHX, or the pump volume, etc. Let the volume of fuel in region i be V_i, and let the neutron source strength in region i be $\overline{S}_i$ neutrons cm^{-3} s^{-1}. Then the reaction rate in region j due to the neutron sources in the various regions of the primary system is given by:

$$R_j=\sum_{i=1}^{N} f_{i\to j} V_i \overline{S}_i \tag{6}$$

where the factor $f_{i\to j}$ is the reaction rate in region j due to one source particle in region i. In this work, the factor $f_{i\to j}$ is calculated with the Monte Carle method.

The task at hand is thus to determine the neutron source density in a region i in the primary system. Consider a packet of fuel traveling through the primary system of the MSR. This packet of fuel will experience a fission rate, depending on the location in the primary system. In the core the fission rate will be high, in other parts of the primary system the fission rate will be (much) lower. The decay of prompt neutrons is very quick, thus in sub-critical regions of the primary system the source of neutrons is due to the decay of delayed neutron precursor nuclei. The precursor concentration increases and decreases as the fuel packet traverses the primary circuit. It is assumed that the packet of fuel is subject to a series of irradiations, each with piece-wise constant fission rate. The entire primary system consists of N such regions, each of length $\tau_i = t_i - t_{i-1}$. Choose $t_0 = 0$ for convenience, then t_N is the recirculation time of the primary system. In each region i, the time rate of change of the precursor density is found as follows (the conventional 6 families of precursors are assumed):

$$\frac{dC_k}{dt}=\beta_k\int_0^\infty \nu\sum_f(E)\varphi(E,t)dE-\lambda_k C_k \tag{7}$$

with C_k the concentration of precursor nuclei of family k, β_k is the delayed neutron fraction, ν the total number of neutrons per fission, $\sum_f$ the fission cross section, φ the scalar flux and λ_k the decay constant.[1] There is a relation between power density and fission rate:

$$\overline{P}=E_r\int_0^\infty \sum_f(E)\varphi(E)dE \tag{8}$$

with E_r the energy released per fission (approx. 3.2×10^{-11} J per fission). Thus, introducing the energy-averaged number of fission neutrons $\overline{\nu}$, one obtains for the production rate of precursors in group k during interval i:

$$\frac{dC_k}{dt}=\beta_k\overline{\nu}\frac{\overline{P}_i}{E_r}-\lambda_k C_k=\alpha_{k,i}-\lambda_k C_k \tag{9}$$

with $\overline{P}_i$ the power density during the i^{th} interval. Note that it is thus not required to explicitly know the fission cross section; one only requires to know the power density to which the fuel is subjected. The above equation can be solved to find the precursor density in the i^{th} interval, subject to the condition that the precursor density is continuous across interval boundaries:

$$C_k(t)=\left[C_k(t_{i-1})-\frac{\alpha_i}{\lambda_k}\right]e^{-\lambda_k(t-t_{i-1})}+\frac{\alpha_i}{\lambda_k} \tag{10}$$

In particular, the precursor density at the end of interval i is found as:

$$C_k(t_i)=\left[C_k(t_{i-1})-\frac{\alpha_i}{\lambda_k}\right]e^{-\lambda_k\tau_i}+\frac{\alpha_i}{\lambda_k} \tag{11}$$

Since the primary circuit is a closed loop, the continuity condition is that $C_k(t_N) = C_k(t_0)$, and Eq. (11) opens the possibility to find a recursive solution to find $C_k(t)$ throughout the primary system if the power density $\overline{P}_i$ in each interval is known. Evaluation of the power density throughout the primary loop requires a solution of the neutron flux in all parts of the primary system, which is not possible at the moment since there is no detailed design of the primary system. Thus, in this work a simplified approach is used, taking 2 intervals, i.e. one interval in the core with $\overline{P}\neq0$ and one interval outside of the core where $\overline{P}=0$; the implicit assumption is that the power density in the fuel salt outside of the core region is negligible. Thus the solution of the precursor density is found as:

$$C_k(t)=\frac{\beta_k}{\lambda_k}\overline{\nu}\frac{\overline{P}}{E_r}\left[1-\frac{e^{-\lambda_k t}(1-e^{-\lambda_k\tau_2})}{1-e^{-\lambda_k(\tau_1+\tau_2)}}\right]\quad\text{in core region} \tag{12}$$

$$C_k(t)=\frac{\beta_k}{\lambda_k}\overline{\nu}\frac{\overline{P}}{E_r}e^{-\lambda_k t}\left[\frac{e^{\lambda_k\tau_1}-1}{1-e^{-\lambda_k(\tau_1+\tau_2)}}\right]\quad\text{out of core region} \tag{13}$$

In general, the fuel packet will enter the IHX at t_i and exit at t_e, spending a time of $\tau_{HX} = t_e - t_i$ in the IHX. Thus one can calculate the average number of precursor decays while the fuel packet traverses the IHX:

$$\overline{S}=\sum_{k=1}^{K}\frac{\lambda_k}{\tau_{HX}}\int_{t_i}^{t_e}C_k(t)dt=\frac{\overline{\nu}\overline{P}}{\tau_{HX}E_r}\sum_{k=1}^{K}\frac{\beta_k}{\lambda_k}\left[\frac{e^{\lambda_k\tau_1}-1}{1-e^{-\lambda_k(\tau_1+\tau_2)}}\right]\times\left(e^{-\lambda_k t_i}-e^{-\lambda_k t_e}\right) \tag{14}$$

Since each precursor decay releases one neutron, the expression of Eq. (14) gives the average neutron source density in the fuel salt while traversing the IHX.

[1] Since one considers region i, it may be better to use the symbol $C_{k,i}$, but for notational simplicity the region index i is suppressed.

4. Results

4.1. The final design of the heat exchanger

The IHX design data is listed in Table 3. The heat exchanger consists of 27×25 helical coil tubes which make 1.75 turns. The inner and outer radii of the tube region are $R_i = 10.0$cm, $R_o = 52.9$cm; the length of the tube region is $H = 277.8$cm. Inlet and outlet plena are assumed above and below the tube region. The height of the plena is $H_p = 30.0$cm. In the plena there are 4 connections for the secondary coolant to connect to the four headers. The heat exchanger coils spiral around a central section. This section is assumed to be made of 80 vol% structural material and 20 vol % coolant. Fig. 2 shows the IHX design. The design found in this work is comparable to the designs presented in [5].

Table 3
The intermediate heat exchanger.

Quantity	Value
Power	150 MW
Tube outside diameter D_o	12.7 mm
Pitch $\delta x = \delta y$	15.875 mm
$NX \times NY$	27×25
Header dimension	$42.9 \times 39.7cm$
Tube region inner radius	10.0 cm
Tube region outer radius	53.0 cm
Tube region length	277.8 cm
Fuel volume in tube region	$0.80m^3$ (34.22 vol%)
Tube volume in tube region	$0.54m^3$ (22.85 vol%)
Coolant volume in tube region	$1.01m^3$ (42.93 vol%)
Fuel volume in plena	$0.25m^3$
Coolant volume in plena	$0.16m^3$
Fuel traversal time	1.6s

4.2. Fuel salt and the primary system

A detailed design of the primary system is not yet available. Since Eq. (14) indicates that the average precursor decay rate depends on the recirculation time as well as the timing of the entrance into the IHX, two designs are considered: one design where the volume of the primary system is twice the core volume, i.e. $V_p = 2V_c$, and one design with $V_p = 5V_c$. These two options are considered to be the limiting cases. Details are given in Table 4 and Fig. 3. In the present work, the delayed neutron parameters were calculated with ERANOS v2.3 [14] with JEFF-3.1 nuclear data; see Table 5. The heavy metal composition is 75 mol% UCl_3 and 25 mol% $PuCl_3$. The isotopic composition of the fuel materials is shown in Table 6. Core power density is set to $\overline{P} = 100\text{MWm}^{-3}$. Other relevant parameters for the primary system are listed in Table 1.

4.3. Monte Carlo modeling

Criticality and reaction rates analyses were performed using the continuous energy Monte Carlo code MVP/GMVP 3 [15] with the

Table 4
Delayed neutron data used in this work.

Parameter	$V_p = 2V_c$	$V_p = 5V_c$
τ_i [s]	2.1	2.1
τ_o [s]	2.1	8.4
t_i [s]	2.3	5.4
t_o [s]	3.9	7.0
τ_{HX} [s]	1.6	1.6
τ_c [s]	4.2	10.5
$\overline{S}$ [s^{-1} cm^{-3}]	1.3273×10^{10}	3.8992×10^{9}

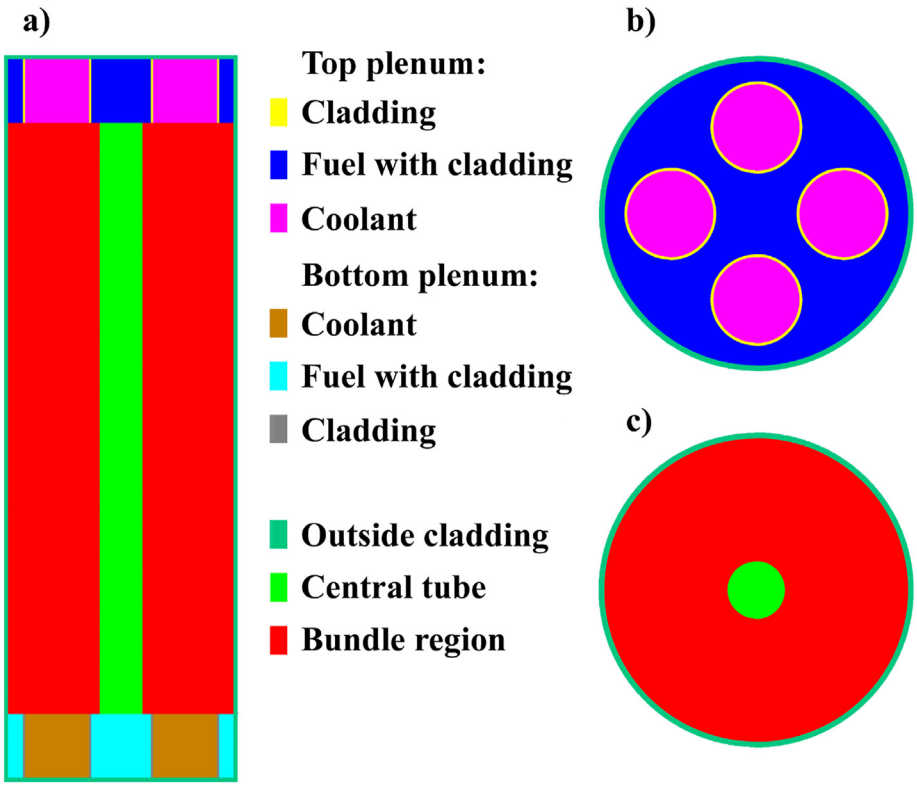

Fig. 2. Illustration of the IHX design. a) Vertical cross section of IHX, b) Horizontal cross section of the top plenum, c) Horizontal cross section of the bundle region.

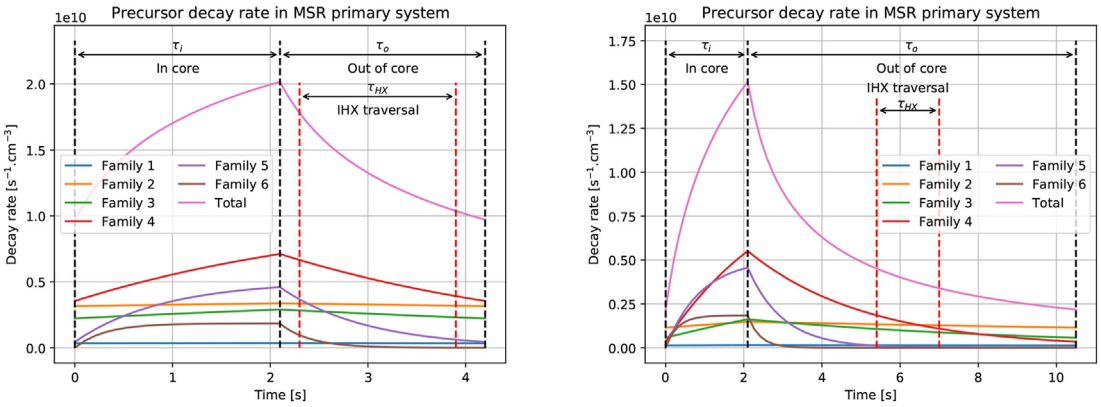

Fig. 3. Illustration of the precursor concentration in the primary circuit of a Molten Salt Reactor assuming a core region with non-zero fission rate and a zero fission rate elsewhere. The traversal of the IHX is also illustrated. Left: $V_p = 2V_c$ case; right: $V_p = 5V_c$ case.

Table 5
Delayed neutron data used in this work.

Group	β_i [pcm]	λ_i [s^{-1}]
1	7.87	0.0131
2	76.1	0.0306
3	59.6	0.126
4	124.0	0.331
5	58.6	1.12
6	21.4	3.27
β	348	

Table 6
Isotopic compositions pertaining to the fuel salt.

Isotope	num%
Light elements	
Cl-35	1.0
Cl-37	99.0
Uranium	
U-234	0.05
U-235	0.05
U-238	99.9
Plutonium	
Pu-238	2.3
Pu-239	53.7
Pu-240	26.7
Pu-241	9.5
Pu-242	7.8

JENDL-4.0 data library [16]. Here the calculation conditions were the same for both eigenvalue and fixed source calculations, as follows: the number of histories per batch was 100,000, the number of batch was 100 and the first 20 batch were neglected for statistical treatments. Calculations were performed with reflective boundary conditions and vacuum boundary conditions; actual conditions will be somewhere in between these two extremes. The material regions in the top and bottom plenum, as well as the tube bundle region are homogeneous. The factor $f_{i\to j}$ was calculated by specifying a source in the top region, or the tube bundle region, or the bottom region; in each case, reaction rates were tallied in the top region, the tube bundle region and the bottom region. For reasons of completeness, the effective multiplication factor k_{eff} was also calculated.

4.4. Reaction rates in the IHX

Results for the fission rate, capture rate and the flux level are given in Table 7, for both reflective boundary conditions and vacuum boundary conditions, based on JENDL-4.0 nuclear data. In the case of the "small" primary circuit, the fission power is about 515 kW in each IHX, thus a total of 2.6 MW for all four IHX; for the "large" primary system, the total power amounts to some 600 kW for four IHX. The capture rate indicates that $k_\infty < 1$ for all studied cases. The neutron flux level is on the order of 3×10^{11} for the vacuum cases to 1×10^{13} for the reflected cases. For the core design presented in this work, the flux level in the core has a maximum value of the order of 1×10^{15}). Thus the flux in the IHX is very much lower than in the core, but a detailed analysis of the component lifetime for the IHX is required. In a typical fast reactor, core structures which are subjected to high flux levels (such as the fuel claddings and subassembly wrapper tubes) have a short residence time, on the order of six months to two years. In the IHX in this work, the flux level is still so high that the lifetime of the components is expected to be limited to (only) several years. For reference, a limited sensitivity study was performed with ENDF/B-VII.0 and JEFF-3.2 nuclear data. The results are presented in the Appendix.

5. Conclusion and discussion

In this work the power production in the Intermediate Heat Exchangers (IHX) of a chloride-fuel based fast-spectrum Molten Salt Reactor has been evaluated. The primary circuit of a Molten Salt Reactor contains the liquid fuel, and thus parameters such as the (averaged) delayed neutron precursor concentration depend on the volume of the primary circuit. For this reason, a "small" primary circuit with $V_p = 2V_c$ and a "large" primary circuit with $V_p = 5V_c$ were analyzed; these volumes are considered to the lower and upper limits for a practical MSR system.

The multiplication factor of the IHX was evaluated to be $k \approx 0.76$ with all reflective boundary conditions, thus deeply subcritical and there is a margin to use larger IHX. Power production in the IHX remains very limited, on the order of 0.1%–0.34% of the primary system power in the case of a fully reflected system. Since the IHX

Table 7
Reaction rates in the IHX, calculations based on JENDL-4.0 nuclear data. Statistical error of the Monte Carlo calculations is given in brackets in units of percent.

Region	Power	Fission	Error	Capture	Error	Flux
	[kW]	Rate [s^{-1}]	[%]	Rate [s^{-1}]	[%]	[cm^{-2} s^{-1}]
$V_p = 2V_c$, reflective BC, $k_{eff} = 0.760095(0.0097\%)$						
Top plenum	66.6	2.0798×10^{15}	(0.0337)	3.7194×10^{15}	(0.0372)	7.0777×10^{12}
Bundle region	382.6	1.1956×10^{16}	(0.0115)	3.1543×10^{16}	(0.0129)	9.0690×10^{12}
Bottom plenum	66.6	2.0817×10^{15}	(0.0314)	3.7228×10^{15}	(0.0357)	7.0831×10^{12}
Total	515.8	1.6117×10^{16}	(0.0180)	3.8985×10^{16}	(0.0197)	
$V_p = 2V_c$, vacuum BC, $k_{eff} = 0.242074(0.0331\%)$						
Top plenum	4.3	1.3540×10^{14}	(0.0948)	1.2572×10^{14}	(0.1347)	5.0394×10^{11}
Bundle region	34.9	1.0901×10^{15}	(0.0162)	2.2013×10^{15}	(0.0235)	9.5291×10^{11}
Bottom plenum	4.3	1.3521×10^{14}	(0.0971)	1.2551×10^{14}	(0.1404)	5.0333×10^{11}
Total	43.5	1.3607×10^{15}	(0.0298)	2.4525×10^{15}	(0.0313)	
$V_p = 5V_c$, reflective BC, $k_{eff} = 0.760095(0.0097\%)$						
Top plenum	19.6	6.1309×10^{14}	(0.0353)	1.0964×10^{15}	(0.0389)	2.0864×10^{12}
Bundle region	112.8	3.5243×10^{15}	(0.0130)	9.2984×10^{15}	(0.0145)	2.6734×10^{12}
Bottom plenum	19.6	6.1366×10^{14}	(0.0309)	1.0974×10^{15}	(0.0351)	2.0880×10^{12}
Total	152.0	4.7511×10^{15}	(0.0213)	1.1492×10^{16}	(0.0225)	
$V_p = 5V_c$, vacuum BC, $k_{eff} = 0.242074(0.0331\%)$						
Top plenum	1.3	3.9912×10^{13}	(0.0948)	3.7061×10^{13}	(0.1347)	1.4855×10^{11}
Bundle region	10.3	3.2134×10^{14}	(0.0162)	6.4890×10^{14}	(0.0235)	2.8090×10^{11}
Bottom plenum	1.3	3.9857×10^{13}	(0.0971)	3.6999×10^{13}	(0.1404)	1.4837×10^{11}
Total	12.9	4.0111×10^{14}	(0.0298)	7.2296×10^{14}	(0.0313)	

has the largest volume of the out-of-core components of the reactor system, neutron multiplication and power production outside of the core region is negligible throughout the MSR primary system.

The capture rate in the IHX is rather low. Although the current work did not specifically evaluate the capture rate in Cl-35 on the secondary side of the IHX, the results indicate that the reaction rate remains limited and enrichment of the chlorine in the secondary system is probably not required.

The neutron flux level in the IHX is (much) lower than the typical flux level in the core of a fast reactor. However, the flux level is still considerable and component lifetime under irradiation must be evaluated.

Declaration of competing interest

The authors declare that they have no known competing financial interests or personal relationships that could have appeared to influence the work reported in this paper.

Acknowledgment

This work was sponsored by the FIHRDC/WERC Accepting Program for Overseas Researchers/Research Students of Atomic Energy JFY2019, of the Wakasa-Wan Energy Research Center, Fukui, Japan, and the Mongolian Foundation for Science and Technology (MEST) 2018/45 project, Ulaanbaatar, Mongolia.

Appendix 1. Results with ENDF/B-VII.0 and JEFF-3.2 nuclear data

To estimate the impact of the nuclear data on the calculated results, the MVP calculations were also performed with two alternative sets of nuclear data, i.e. cross sections libraries based on ENDF/B-VII.0, and on JEFF-3.2. Results are given in Tables 8 and 9

Table 8
Reaction rates in the IHX, calculations based on ENDF/B-VII.0 nuclear data. Statistical error of the Monte Carlo calculations is given in brackets in units of percent.

Region	Power	Fission	Error	Capture	Error	Flux
	[kW]	Rate [s^{-1}]	[%]	Rate [s^{-1}]	[%]	[cm^{-2} s^{-1}]
$V_p = 2V_c$, reflective BC, $k_{eff} = 0.757516(0.0080\%)$						
Top plenum	65.8	2.0559×10^{15}	(0.0353)	3.6161×10^{15}	(0.0389)	7.0396×10^{12}
Bundle region	378.4	1.1825×10^{16}	(0.0130)	3.1317×10^{16}	(0.0145)	9.0292×10^{12}
Bottom plenum	65.8	2.0564×10^{15}	(0.0309)	3.6166×10^{15}	(0.0351)	7.0409×10^{12}
Total	510.0	1.5937×10^{16}	(0.0213)	3.8550×10^{16}	(0.0225)	
$V_p = 2V_c$, vacuum BC, $k_{eff} = 0.235474(0.0364\%)$						
Top plenum	4.2	1.3228×10^{14}	(0.0973)	1.1950×10^{14}	(0.1418)	4.9516×10^{11}
Bundle region	33.8	1.0578×10^{15}	(0.0164)	2.1701×10^{15}	(0.0225)	9.3285×10^{11}
Bottom plenum	4.2	1.3221×10^{14}	(0.0977)	1.1947×10^{14}	(0.1401)	4.9480×10^{11}
Total	41.2	1.3223×10^{15}	(0.0303)	2.4091×10^{15}	(0.0322)	
$V_p = 5V_c$, reflective BC, $k_{eff} = 0.757516(0.0080\%)$						
Top plenum	19.4	6.0606×10^{14}	(0.0353)	1.0660×10^{15}	(0.0389)	2.0752×10^{12}
Bundle region	111.5	3.4857×10^{15}	(0.0130)	9.2317×10^{15}	(0.0145)	2.6617×10^{12}
Bottom plenum	19.4	6.0620×10^{14}	(0.0309)	1.0661×10^{15}	(0.0351)	2.0755×10^{12}
Total	150.3	4.6979×10^{15}	(0.0213)	1.1364×10^{16}	(0.0225)	
$V_p = 5V_c$, vacuum BC, $k_{eff} = 0.235474(0.0364\%)$						
Top plenum	1.2	3.8995×10^{13}	(0.0973)	3.5227×10^{13}	(0.1418)	1.4597×10^{11}
Bundle region	9.9	3.1181×10^{14}	(0.0164)	6.3972×10^{14}	(0.0225)	2.7499×10^{11}
Bottom plenum	1.2	3.8972×10^{13}	(0.0977)	3.5218×10^{13}	(0.1401)	1.4586×10^{11}
Total	12.3	3.8978×10^{14}	(0.0303)	7.1017×10^{14}	(0.0322)	

Table 9
Reaction rates in the IHX, calculations based on JEFF-3.2 nuclear data. Statistical error of the Monte Carlo calculations is given in brackets in units of percent.

Region	Power	Fission	Error	Capture	Error	Flux
	[kW]	Rate [s^{-1}]	[%]	Rate [s^{-1}]	[%]	[cm^{-2} s^{-1}]
$V_p = 2V_c$, reflective BC, $k_{eff} = 0.764822(0.0082\%)$						
Top plenum	67.3	2.1046×10^{15}	(0.0346)	3.7248×10^{15}	(0.0386)	7.2807×10^{12}
Bundle region	392.9	1.2279×10^{16}	(0.0128)	3.2014×10^{16}	(0.0142)	9.4715×10^{12}
Bottom plenum	67.4	2.1051×10^{15}	(0.0322)	3.7257×10^{15}	(0.0360)	7.2832×10^{12}
Total	537.6	1.6489×10^{16}	(0.0201)	3.9465×10^{16}	(0.0175)	
$V_p = 2V_c$, vacuum BC, $k_{eff} = 0.234398(0.0302\%)$						
Top plenum	4.2	1.3224×10^{14}	(0.0965)	1.1632×10^{14}	(0.1416)	4.9069×10^{11}
Bundle region	33.6	1.0499×10^{15}	(0.0165)	2.0629×10^{15}	(0.0224)	9.2394×10^{11}
Bottom plenum	4.2	1.3229×10^{14}	(0.0958)	1.1645×10^{14}	(0.1342)	4.9080×10^{11}
Total	42.0	1.3144×10^{15}	(0.0203)	2.2961×10^{15}	(0.0332)	
$V_p = 5V_c$, reflective BC, $k_{eff} = 0.764822(0.0082\%)$						
Top plenum	19.9	6.2040×10^{14}	(0.0346)	1.0980×10^{15}	(0.0386)	2.1462×10^{12}
Bundle region	115.8	3.6198×10^{15}	(0.0128)	9.4372×10^{15}	(0.0142)	2.7920×10^{12}
Bottom plenum	19.9	6.2055×10^{14}	(0.0322)	1.0983×10^{15}	(0.0360)	2.1470×10^{12}
Total	155.6	4.8607×10^{15}	(0.0201)	1.1634×10^{16}	(0.0175)	
$V_p = 5V_c$, vacuum BC, $k_{eff} = 0.234398(0.0302\%)$						
Top plenum	1.2	3.8983×10^{13}	(0.0965)	3.4289×10^{13}	(0.1416)	1.4465×10^{11}
Bundle region	9.9	3.0949×10^{14}	(0.0165)	6.0812×10^{14}	(0.0224)	2.7236×10^{11}
Bottom plenum	1.2	3.8998×10^{13}	(0.0958)	3.4328×10^{13}	(0.1342)	1.4468×10^{11}
Total	12.3	3.8747×10^{14}	(0.0203)	6.7673×10^{14}	(0.0332)	

References

[1] Ondřej Beneš, Thermodynamics of Molten Salts for Nuclear Applications, PhD thesis, Institute of Chemical Technology Prague, 2008. URL, https://publications.jrc.ec.europa.eu/repository/bitstream/JRC50490/ReqNo_JRC50490_Benes.pdf.

[2] Suddhasattwa Ghosh, B. Prabhakara Reddy, K. Nagarajan, K.C. Hari Kumar, Experimental investigations and thermodynamic modelling of KCl-LiCl-UCl_3 system, CAL 45 (2014) 11–26, https://doi.org/10.1016/j.calphad.2013.11.001.

[3] Mariya Brovchenko, Jan-Leen Kloosterman, Lelio Luzzi, Elsa Merle, Daniel Heuer, Axel Laureau, Olga Feynberg, Victor Ignatiev, Manuele Aufiero, Antonio Cammi, Carlo Fiorina, Fabio Alcaro, Sandra Dulla, Piero Ravetto, Lodewijk Frima, Danny Lathouwers, Merk Bruno, Neutronic benchmark of the molten salt fast reactor in the frame of the EVOL and MARS collaborative projects, EPJ Nuclear Science and Technologies 5 (2) (2019), https://doi.org/10.1051/epjn/2018052.

[4] Delphine Gérardin, Anna Chiara Uggenti, Stéphane Beils, Andrea Carpignano, Sandra Dulla, Elsa Merle, Daniel Heuer, Axel Laureau, Michel Allibert, A methodology for the identification of the postulated initiating events of the molten salt fast reactor, Nuclear Engineering and Technology 51 (4) (2019) 1024–1031, https://doi.org/10.1016/j.net.2019.01.009.

[5] Andrea Di Ronco, Antonio Cammi, Stefano Lorenzi, Preliminary analysis and design of the heat exchangers for the molten salt fast reactor, Nuclear Engineering and Technology 52 (2020) 51–58, https://doi.org/10.1016/j.net.2019.07.013.

[6] Guangxuan Lu, Christian Robelin, Patrice Chartrand, Maogang He, Kun Wang, Thermodynamic evaluation and optimization of the (LiCl + NaCl + KCl + $MgCl_2$ + $CaCl_2$ + $CeCl_3$) system, Fluid Phase Equil. 487 (2019) 83–97, https://doi.org/10.1016/j.fluid.2018.11.031.

[7] George J. Janz, Molten Salts Handbook, Academic Press, 1967.

[8] Toni Y. Karlsson, Guy L. Fredrickson, Tae-Sic Yoo, DeeEarl Vaden, Michael N. Patterson, Vivek Utgikar, Thermal analysis of projected molten salt compositions during FFTF and EBR-II used nuclear fuel processing, J. Nucl. Mater. 520 (2019) 87–95, https://doi.org/10.1016/j.jnucmat.2019.04.016.

[9] B. Cliff, Davis. Implementation of Molten Salt Properties into RELAP5-3D/ATHENA. Technical Report INEEL/EXT-05-02658, Idaho National Engineering and Environmental Laboratory, January 2005. URL, https://inldigitallibrary.inl.gov/sites/STI/STI/3028316.pdf.

[10] R. Serrano-López, J. Fradera, S. Cuesta-López, Molten salts database for energy applications, Chem. Eng. Process: Process Intensification 73 (2013) 87–102, https://doi.org/10.1016/j.cep.2013.07.008.

[11] Theodore L. Bergman, Adrienne S. Lavine, Frank P. Incropera, David P. Dewitt, Fundamentals of Heat and Mass Transfer, seventh ed. edition, John Wiley and Sons, 2011.

[12] Salzgitter Mannesmann Precision, Cold drawn seamless heat exchanger tubes for process industries, Available online, Accessed in 2020. URL, https://www.mannesmann-precision-tubes.com/img/Downloads_Prospekte_2011/SMP_Heat_Exchanger_Tubes.pdf.

[13] A. Žukauskas, Heat transfer from tubes in crossflow, Adv. Heat Tran. 8 (1972) 93–160, https://doi.org/10.1016/S0065-2717(08)70038-8.

[14] D. Plisson-Rieunier, Description of the ERANOS 2.3N Release. Technical Report DER/SPRC/LEDC 13-419 IND A, CEA, 2013.

[15] Y. Nagaya, K. Okumura, T. Mori, et al., MVP/GMVP Version 3: General Purpose Monte Carlo Code for Neutron and Photon Transport Calculations Based on Continuous Energy and Multigroup Methods. JAEA-Data/Code 2016-018, Japan Atomic Energy Agency, 2017.

[16] K. Shibata, O. Iwamoto, T. Nakagawa, et al., JENDL-4.0: A New Library for Nuclear Science and Engineering, 2011.